Fotovoltaik Güneş Panelleri için Pasif Soğutmalı Isı Kuyusunun Tasarımı, Simülasyonu ve Deneysel Analizi

Design, Simulation and Experimental Analysis of a Passive Cooling Heat Sink for Photovoltaic Solar Panels

Feyzullah Behlül Özkul[1] , **Fatih Mehmet Ulu[1]** , **Erhan Kayabaşı[1]**

[1]Karabük Üniversitesi, Makina Mühendisliği Bölümü, 78050 KARABÜK, TÜRKİYE

Öz

Bu araştırmada, fotovoltaik (PV) panellerin soğutma verimliliğini artırma amacıyla yeni bir termal yönetim çözümü tasarlandı. İlk olarak, kanatçık yapılandırmalarını değerlendirmek için ANSYS yazılımı kullanılarak bir simülasyon çalışması yürütüldü. Simüle edilen veriler kullanılarak, daha düşük sıcaklık değeri sağlayan en avantajlı tasarımı seçildi ve doğrulama aşaması deneylerle gerçekleştirildi. Bu aşamada, ısı kuyusu eklenmiş ve ısı kuyusuz olmak üzere iki PV panel ile atmosfer şartlarında deneyler eş zamanlı olarak gerçekleştirildi. Sıcaklık dağılımları, elektrik çıkışı ve operasyonel verimlilik gibi temel performans ölçütleri kısa zaman aralıkları ile kaydedildi. PV panellerinin sıcaklık, voltaj ve akım değerleri 10:00 ile 16:00 arasında 20 dakikalık aralıklarla ölçüldü ve kaydedildi. Sonuç olarak, HS ile donatılmış güneş panelinin, HS'siz PV paneline göre gün boyunca %15-21,5 oranında daha verimli çalıştığı gözlemlenmiştir.

Anahtar Kelimeler

PV Panel, Pasif Soğutma, Isı Emici, CFD analizi

Abstract

In this investigation, a novel thermal management solution was engineered for the purpose of enhancing the cooling efficiency of photovoltaic (PV) panels. First, a simulation study was conducted utilizing ANSYS software to evaluate fin configurations. Building upon the simulated data, a prototype reflecting the most advantageous design that is providing the less temperature values was selected the validation stage was performed by experiments. This phase employed two distinct PV panels: one interfaced with the fabricated heat sink (HS) and the other devoid of any thermal management system. Key performance metrics such as thermal gradients, electrical output, and operational efficiency were meticulously recorded. The temperature, voltage and current values of the PV panels were measured and recorded at 20-minute intervals from 10:00 to 16:00. As a result, it was observed that the solar panel equipped with a HS worked 15-21.5 % more efficiently throughout the day than the PV panel without a HS.

Key Words

PV Panel, Passive Cooling, Heat Sink, CFD analysis

1. Introduction

Photovoltaic solar cells manufactured using silicon semiconductors are a very useful energy conversion option for converting solar energy directly into electrical energy[1]. In addition, the silence and less emissivity features of PV panels make it environmentally friendly [2,3]. Solar energy is a crucial element of renewable energy technologies and is essential for addressing the global energy deficit. As one of the key renewable energy sources, solar power plays a pivotal role in the decarbonization of buildings. In regions with ample solar resources, residential areas have the potential to evolve into self-sustaining, smart communities [4]. Depending on the region where PV panels operate, there are some environmental factors that negatively affect their efficiency, such as high temperatures and pollution [5]. There are quite easy and common cleaning options in the industry for cleaning PV panel [6].

However, there is still no generalized solution for keeping the panel temperature close to the test conditions and achieving a homogenized temperature distribution on the panel surface [7]. In the literature, cooling of PV panels is examined under two main headings: Active cooling and Passive cooling [8]. In active cooling systems, forced convection is generally used to cool PV panels and the method also requires energy consumption. However, passive cooling methods are carried out using passive additions that increase the heat transfer surface and do not require energy consumption. Wind cooling, cooling with natural convection with water over rivers and oceans, HSs, natural moisture, soil covered copper plates, thermoelectric options can be counted as passive cooling methods [9,10]. Through them, passive cooling is the first method that comes to mind with natural convection cooling method. In a study by Kayabasi (2018), the impact of various cooling methods on the efficiency of photovoltaic (PV) panels was investigated. The methods analyzed included natural convection cooling, water cooling, and HS cooling systems. The study found that the PV panel surface temperature could be reduced to 62°C with a passive air velocity of 2.5 m/s. Using water cooling, the temperature dropped to 35°C with a water flow rate of 0.03 kg/s, although this method required energy input to maintain water circulation, thus consuming some of the generated energy. The HS cooling method achieved a surface temperature of 38°C under natural convection conditions, maintaining a stable temperature even at low wind speeds [11]. Skeih et al. (2024), studied a passive multi-layered PCMs cooling system numerically. They reached an efficiency increase of 5% and kept the temperature of PV panel below 60 °C using multilayered PCM systems[12]. Hamed et al. (2024) researched concentrated PV using adsorption/desorption and heat sink cooling methods experimentally. They performed their experiment with three configurations of adsorption/desorptions and metal heat sinks for CPV cooling. They revealed that the combination of a heat sink and silica gel bed, performs best with an average PV temperature reduction of 9.8 °C and enhanced generated power of 29.8 % [13].

Rahimi et al. (2015) compared single and multi-concept cooling methods, finding that the multi-concept approach improved surface temperature by 6.8% and efficiency by 28% [14]. Idoko et al. (2018) studied a multi-concept cooling method combining conductive, air, and water cooling in Nigeria, using 250W PV panels. They observed a 5°C temperature reduction and a 3% efficiency increase[9]. Soliman et al. (2018) used HS cooling with halogen lamps to simulate solar radiation in a lab, achieving a 5.4% temperature decrease and an 8% efficiency increase without additional energy input [15]. Peter Atkin and Mohammed Farid (2015) incorporated PCM with a HS, using MATLAB and performing experiments [2]. Al-Waeli et al. explored the use of SiC nanofluid, containing 3 wt. % nanoparticles, as a cooling fluid for PV panels, resulting in up to a 24.1% efficiency increase and an 8.24% temperature drop with various nanofluids and nanoparticle concentrations [16]. When the literature is examined, PV panel temperature management systems generally focus on active cooling methods. However, it is observed that passive cooling systems of PV panels, simulations of suitable HS designs and experimental analysis are insufficient.

In this study three distinctive HSs were designed employing SpaceClaim and CFD analysis was performed using ANSYS Fluent under different flow velocities and different flow directions. The most effective design giving the less temperature values was chosen depending on the simulation results and used in the experimental stage. As a result, approximately 20% efficiency increase was observed without any additional energy consumption.

2. Materials and Methods

In this study, a unique approach was brought to the HS cooling, which is one of the passive cooling techniques, and a numerical and experimental study was carried out on the design by working on various parameters with a new design and layout. Afterwards, the HS was manufactured of aluminum and mounted on the PV panel experimental setup. The HS was mounted on one of the two PV panels in the test setup using thermal paste. The temperature distribution, current and voltage values were recorded simultaneously for both PV panels. The efficiency of the solar panels was calculated using the obtained values and compared with the temperature values of the PV panel and the simulation results. The experiments were carried out on the roof of the Iron and Steel Institute located in Karabük University Campus (41.2° N, 32.65°E, Time zone: UTC+03, Europe/Istanbul) and the radiation values of this region were taken as reference in the simulation. The radiation and sun angle of the experiment location are shown in Fig. 1.
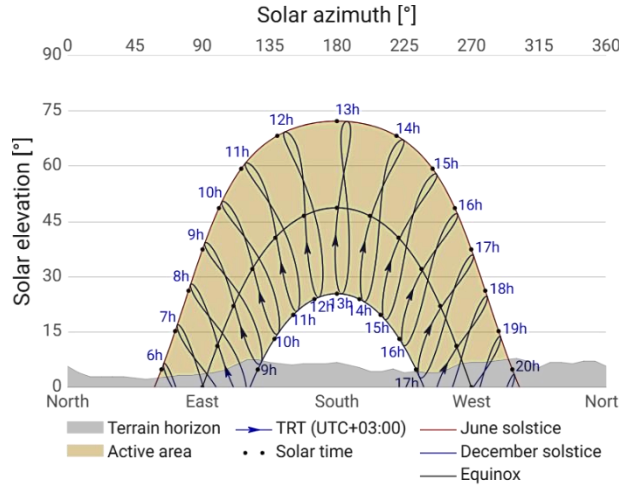
Figure 1. Solar azimuth and angle curves of the experiment zone.

The hourly and monthly radiation averages at the experiment place are presented in Fig. 2. The hourly and monthly radiation average values at the specified location are presented in Fig. 2. Experimental studies were carried out on October 2, between 10:00 and 16:00 [17].

	Jan	Feb	Mar	Apr	May	Jun	Jul	Aug	Sep	Oct	Nov	Dec
4 - 5					1	18						
5 - 6				7	96	161	136	55	1			
6 - 7			31	138	230	284	322	274	167	47		
7 - 8		64	173	251	327	389	453	418	330	194	89	
8 - 9	164	215	259	336	411	487	560	534	436	293	253	166
9 - 10	229	281	328	405	477	556	628	617	520	382	336	232
10 - 11	267	334	366	441	505	578	655	661	563	436	396	271
11 - 12	284	351	377	432	500	560	645	652	559	451	423	287
12 - 13	288	348	374	404	461	513	613	614	536	440	422	292
13 - 14	278	335	350	373	424	467	573	560	490	416	394	279
14 - 15	249	315	330	336	369	424	535	505	441	366	339	244
15 - 16	177	261	271	289	329	382	486	455	380	279	205	115
16 - 17	21	119	198	235	273	345	431	385	285	56		
17 - 18			29	109	208	294	355	259	44			
18 - 19					31	101	105					
Sum	1,956	2,622	3,087	3,757	4,643	5,558	6,497	5,990	4,752	3,360	2,856	1,885

Figure 2. Average solar radiation distribution of the experiment zone [17].

2.1. CFD Simulations

In CFD simulations, different types of HSs and air flow velocities of 1 m/s, 1.5 m/s, and 3 m/s in both horizontal and vertical directions were modeled. The mass, momentum, and energy equations were solved using ANSYS Fluent. As shown in Eq. 1, the software solved the conservation of mass equations during the simulation.

$$\frac{\partial \rho}{\partial t} + \nabla \cdot (\rho \vec{v}) = S_m \tag{1}$$

Where S_m represents the mass change for both compressible and incompressible flows, ρ is the density (kg/m³), $\vec{v}$ is the fluid velocity, and ∇ denotes divergence. Simultaneously, energy conservation was calculated using Eq. 2.

$$\left(u\frac{\partial T}{\partial x} + v\frac{\partial T}{\partial y} + w\frac{\partial T}{\partial z}\right) = \alpha \left(u\frac{\partial^2 T}{\partial x^2} + v\frac{\partial^2 T}{\partial y^2} + w\frac{\partial^2 T}{\partial z^2}\right) \tag{2}$$

Where u, v, and w are the velocity components in the x, y, and z directions, respectively, and α is the thermal emission coefficient. The conservation of momentum calculations is shown in Eq. 3.

$$\frac{\partial}{\partial t}(\rho \vec{v}) + \nabla \cdot (\rho \vec{v} \vec{v}) = \nabla p + \nabla \cdot (\bar{\bar{\tau}}) + \rho g + \vec{F} \tag{3}$$

Here, P is the static pressure, $\bar{\bar{\tau}}$ is the stress tensor, ρg is gravitational body force and F is external body forces.

In Eq. 3, stress tensor calculation formula was given to be used in Eq. 4.

$$\bar{\bar{\tau}} = \mu \left[(\nabla \vec{v} + \nabla \vec{v}^T) - \frac{2}{3}\nabla \cdot \vec{v} I \right] \tag{4}$$

Where, μ is molecular viscosity, I is unit tensor, ∇ is divergence, $\vec{v}$ is velocity of fluid $\bar{\bar{\tau}}$ is the stress tensor. Reynolds number were calculated by using Eq. 5 [3].

$$Re_L = \frac{u_m L}{\nu} \tag{5}$$

When the flow was identified as turbulent, additional module selections were required. The k-epsilon for calculation model was chosen, and the required parameters were configured to enhance the precision of the simulations. Following by setting these parameters, the calculations were done and converged after 260 iterations.

2.2. Experimental Studies

In the experiment, 20 W powered two identical PV panels, 4 multimeters and 2 bulbs were used as is seen in Fig. 3.
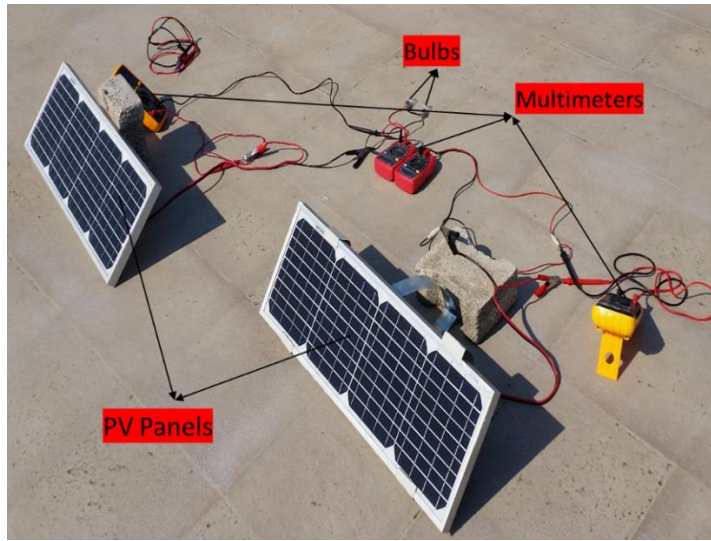
Figure 3. Experimental setup.

Initially, the PV panels were positioned identically in terms of the same radiation conditions. Subsequently, two multimeters identical properties were used to measure the voltage output, and another two identical multimeters were employed to measure the current output of the TPS-1055 Mono Crystalline PV panel. Both PV panels' temperature distribution was monitored by 20 minutes interval and peak temperatures were recorded. PV panel module properties were listed in Table 1.

Table 1. PV panel properties used in the experiments.

Parameter	Quantity	Unit
Maximum Power (P_{max})	20	W_p
Open Circuit Voltage (V_{oc})	22.32	V
Short Circuit Current (I_{sc})	1.13	A
Maximum Power Voltage (V_{mp})	18.0	V
Maximum Power Current (I_{mp})	1.11	A

Power input values calculated using Eq. 6.

$$P_{in} = IA \tag{6}$$

Here, I is the irradiance and A is the surface area of PV panels. Fill Factor was calculated using Eq.7.

$$FF = \frac{P_{max}}{V_{oc}I_{sc}} \tag{7}$$

The Fill Factor value is used to determine the operating efficiency of a PV panel. The efficiency of a PV panel under ideal conditions can be calculated using Eq. 8.

$$\eta = \frac{V_{oc}I_{sc}FF}{P_{in}} \tag{8}$$

Both the open circuit voltage and the fill factor exhibit a significant reduction with increasing temperature, primarily due to the dominance of thermally excited charge carriers influencing the electrical characteristics of the semiconductor. In contrast, the short-circuit current shows a slight increase with temperature [18]. Thus, it is possible to calculate the linear change of the effect of temperature on efficiency with the equation as in Eq. 9.

$$\eta = \eta_{Tref}[1 - \beta_{ref}(T_c - T_{Tref})] \tag{9}$$

Where, η_{Teff} is calculated efficiency, β_{ref} is temperature coefficient ($\approx$ 0.0045 K-1 for Si crystals), Tc is operating temperature, T_{ref} is reference temperature at reference efficiency. The values of η_{Tref} and β_{ref} are typically provided by the photovoltaic (PV) manufacturer. However, they can also be determined through flash tests, where the electrical output of the module is measured at two different temperatures under a constant solar radiation flux. The precise value of the temperature coefficient depends not only on the PV material but also on T_{ref} and is defined by the ratio presented in Eq. 10.

$$\beta_{ref} = \frac{1}{T_o - T_{ref}} \tag{10}$$

Where, T_0 is the temperature at zero efficiency is seen at 270 °C for c-Si [19].

2.3. Heat Sink Design

During the HS design phase, 3 different designs were focused on: regular HS, center-break HS and perforated HS. The regular row HS was selected as the starting point during the design and then the corners of the HS fins were broken to prevent flow turbulence during the flow entry phase and the fin heights were changed to increase from the edge to the middle. Finally, holes were opened on the second design to improve vertical flow conditions, and it was aimed to ensure that cooling can continue efficiently when the wind direction changes.
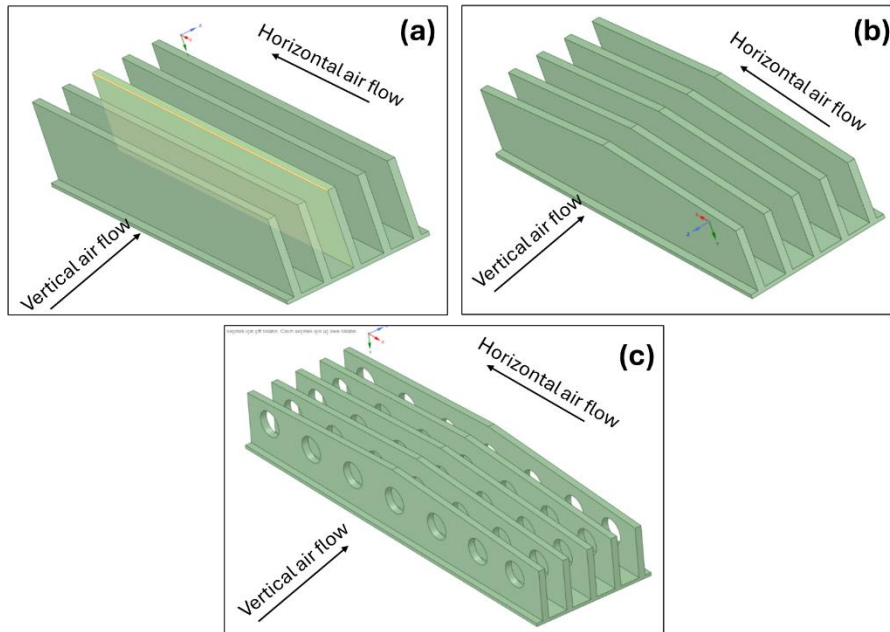

Figure 4. Design options: **a)** flat, **b)** modified flat, **c)** modified with holes

HS designs were developed in the ANSYS SpaceClaim module. During the meshing process, the skewness mesh metrics spectrum was used to ensure the skewness value was within an acceptable range, which was recorded as 0.94 in the quality section.

Next, the Reynolds number was calculated, and the simulation configuration was set based on the flow created by the wind in both horizontal and vertical directions. Simulations were conducted at air velocities of 1 m/s, 1.5 m/s, and 3 m/s for both flow directions.

3. Results and Discussion

In Figure 5, simulation results for horizontal flow at 1 m/s, 1.5 m/s and 3 m/s for a flat HS are given. When Figure 5 is examined, it is observed that the highest temperature on the HS for an air flow rate of 1 m/s is 51.3 C, for 1/5 m/s it is 46.7 C and for 3 m/s it is 40 C. It is expected that the increase in the flow rate decreases the peak temperature on the HS and the option with the highest flow rate shows the best performance. Here the air flow is horizontal, and the flow easily occurs between the HS fins. When the flow is in the vertical direction, the results can be examined in Figure 8. Here it is seen that the peak temperature on the HS increases to 54.7 C for a flow rate of 1 m/s. This situation is observed to be 49.7 C for a flow rate of 1.5 m/s and 41.1 C for 3 m/s. Thus, it is understood that an improvement is required in the HS when the flow direction changes in the HS. Because it is observed

that the air flow cannot reach the fins in vertical flow, and it is observed that the fins and surfaces after the leading fin are at higher temperatures.
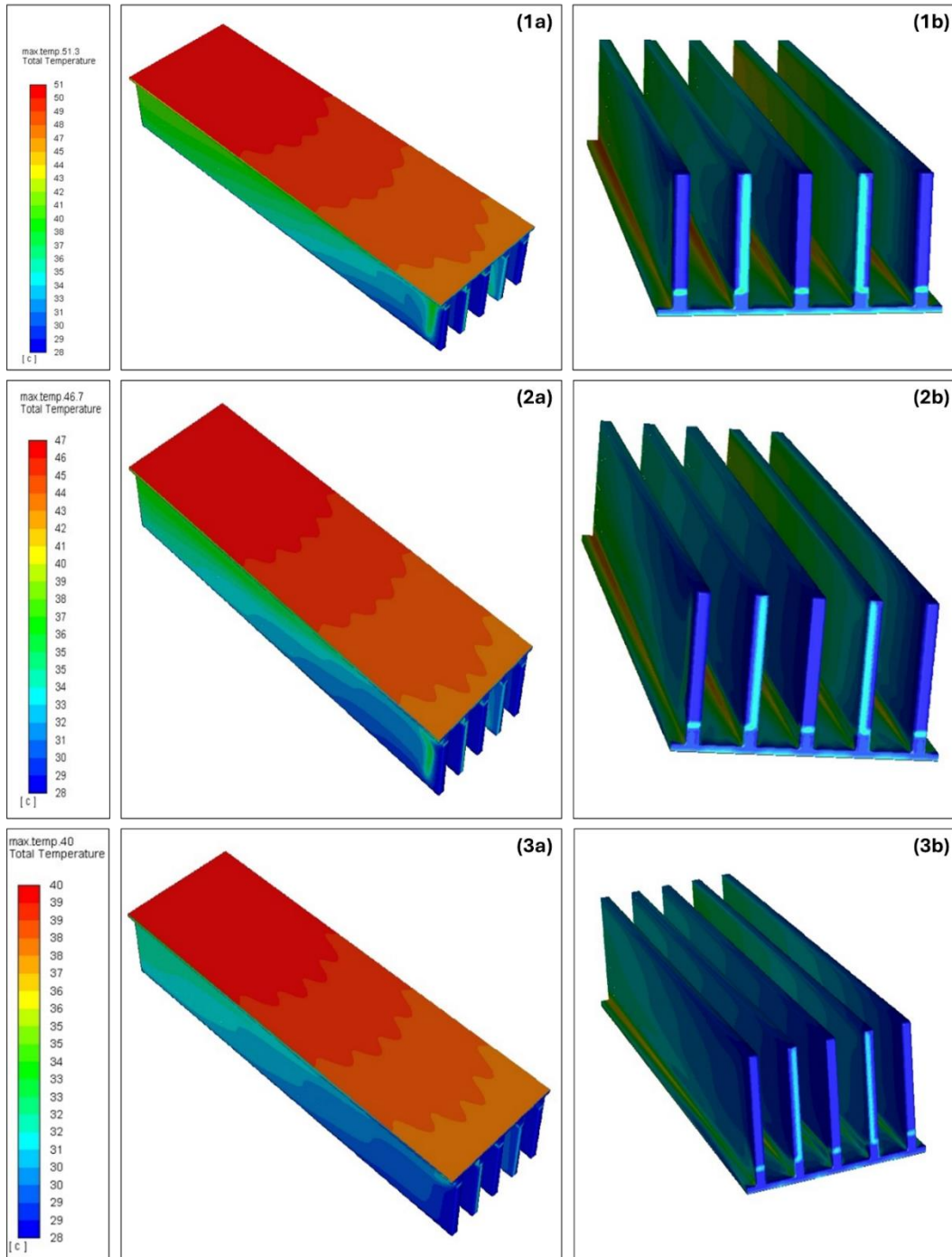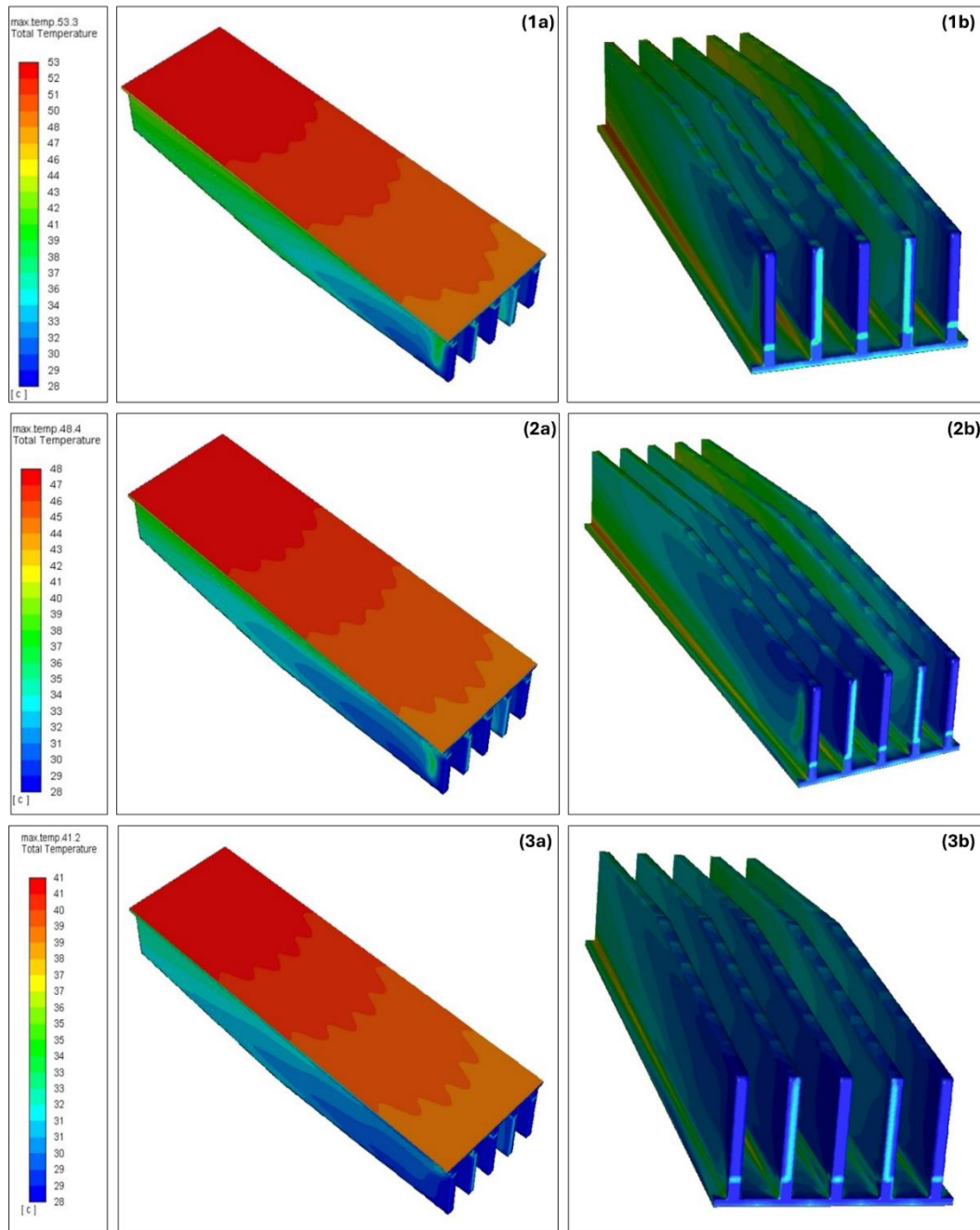

Figure 5. Temperature distribution of flat HS design under horizontal air flow: 1: 1m/s, 2: 1.5 m/s, 3: 3 m/s, **a)** top, **b)** bottom.

In Figure 6, simulation results for horizontal flow at 1 m/s, 1.5 m/s and 3 m/s for a modified flat HS are given. When Figure 6 is examined, it is observed that the highest temperature on the HS for an air flow rate of 1 m/s is 53.3 C, for 1/5 m/s it is 48.4 C and for 3 m/s it is 41.2 C. Here the air flow is horizontal, and the flow easily occurs between the HS fins like the first option. When the flow is in the vertical direction, the results can be examined in Figure 9. Here it is seen that the peak temperature on the HS increases to 57 C for a flow rate of 1 m/s. This situation is observed to be 47.1 C for a flow rate of 1.5 m/s and 42.1 C for 3 m/s. Thus, it is understood the modified HS showed weaker performance in terms of peak temperature.

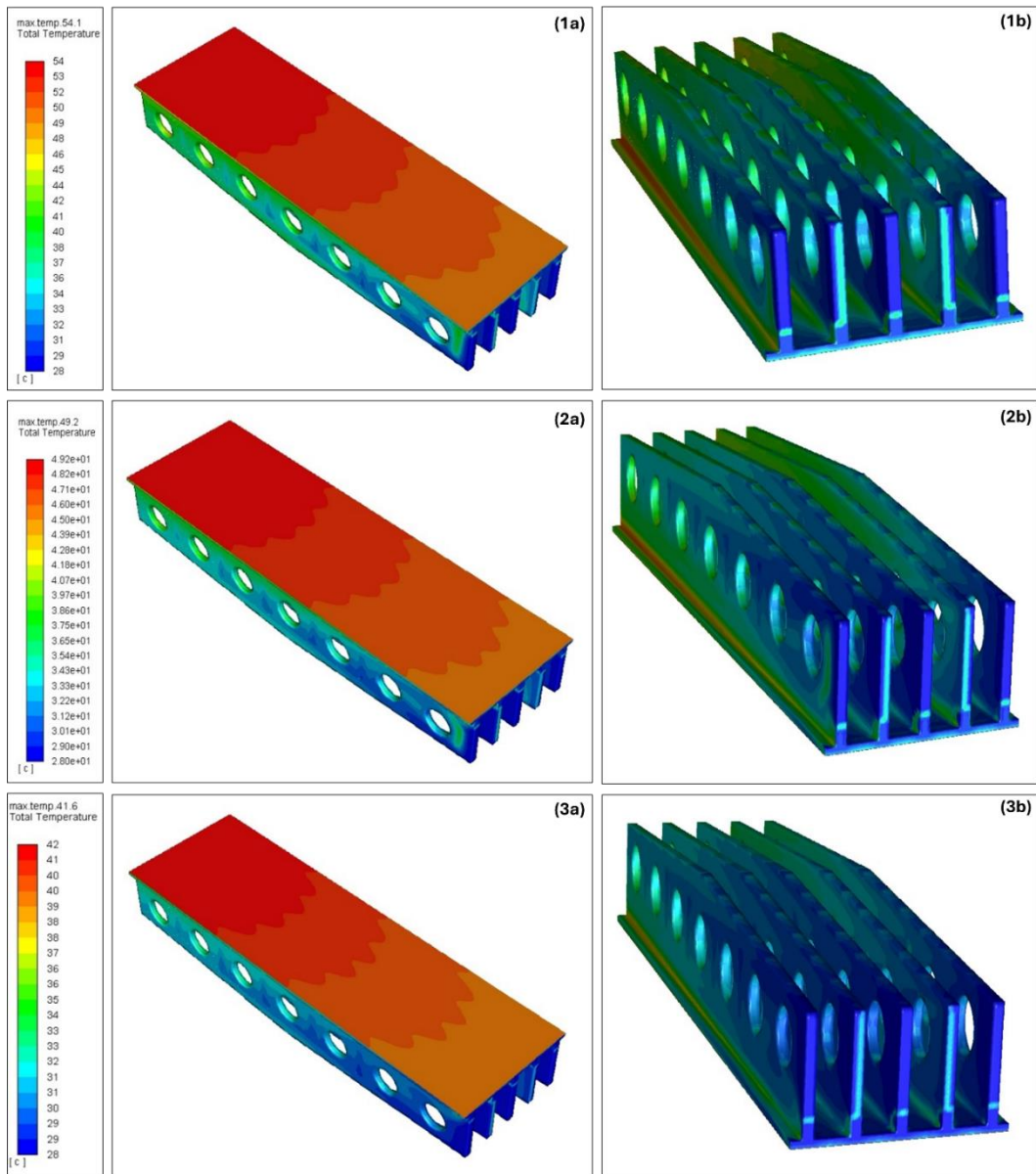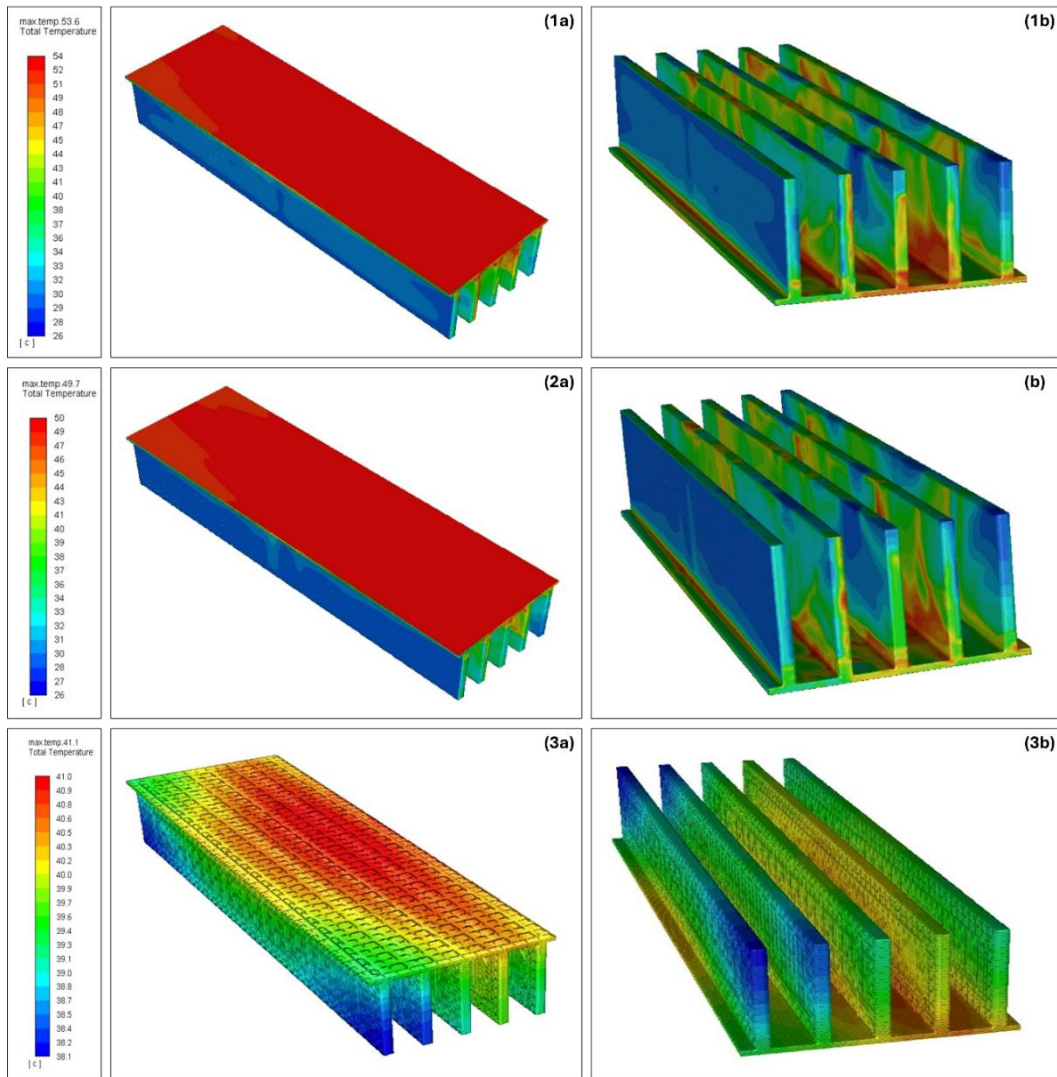**Figure 6.** Temperature distribution of knuckled HS design under horizontal air flow: 1: 1m/s, 2: 1.5 m/s, 3: 3 m/s, **a)** top, **b)** bottom.

In Figure 7, simulation results for horizontal flow at 1 m/s, 1.5 m/s and 3 m/s for a modified flat HS with holes are given. When Figure 8 is examined, it is observed that the highest temperature on the HS for an air flow rate of 1 m/s is 54.1 C, for 1/5 m/s it is 49.2 C and for 3 m/s it is 41.6 C. The results are close to the first two options. When the flow is in the vertical direction, the results can be examined in Figure 10. Here it is seen that the peak temperature on the HS increases to 54 C for a flow rate of 1 m/s. This situation is observed to be 49.6 C for a flow rate of 1.5 m/s and 40.1 C for 3 m/s. Thus, it is understood the modified HS with holes showed better performance in terms of peak temperature.

Figure 7. Temperature distribution of knuckled with holes HS design under horizontal air flow: 1: 1m/s, 2: 1.5 m/s, 3: 3 m/s, **a)** top**, b)** bottom.

The results show that the first option out of three designs provides lower temperatures for horizontal flow at all three flow rates. In other words, it has been proven that changing the angle of the fins or opening holes on them in horizontal flow will not have a positive effect on cooling the PV panel. Therefore, when the PV panel is installed in a region where the flow direction is mostly horizontal, using unmodified flat fins will be the best option in terms of both temperature distribution and ease of production.
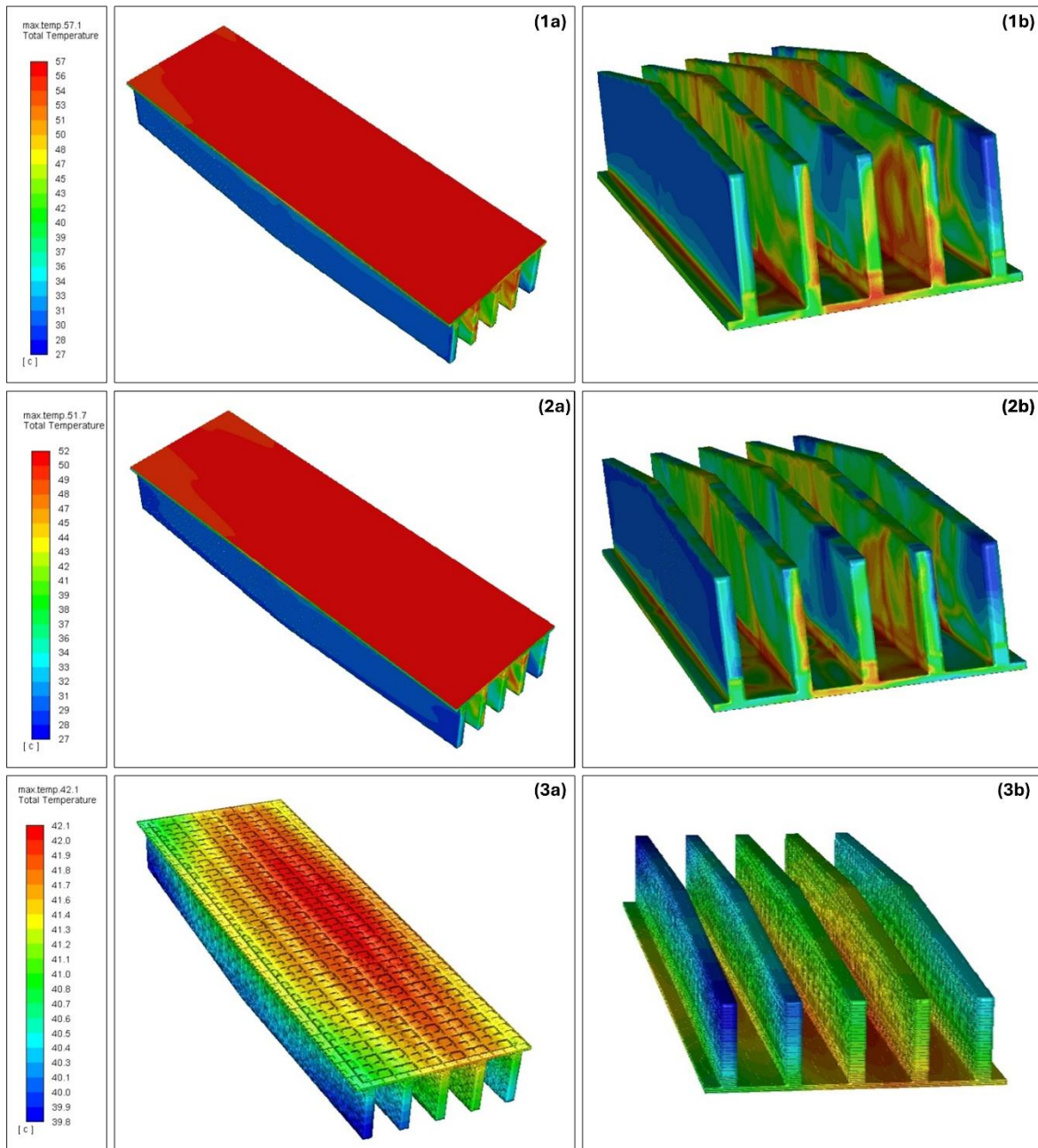
Figure 8. Temperature distribution of flat HS design under vertical air flow: 1: 1m/s, 2: 1.5 m/s, 3: 3 m/s, **a)** top, **b)** bottom.

When the flow direction is vertical, it is observed that the temperature values of the first regular HS at a flow rate of 1 m/s are almost the same as the perforated inclined HS. However, when the flow rate reaches 3 m/s, it is observed that the perforated inclined HS drops to lower temperatures. This shows that the inclined perforated HS provides better heat transfer at high air flow rates. In addition, it is seen from the simulation results that the inclined modified HS option performs lower than the others in all temperature and flow directions.
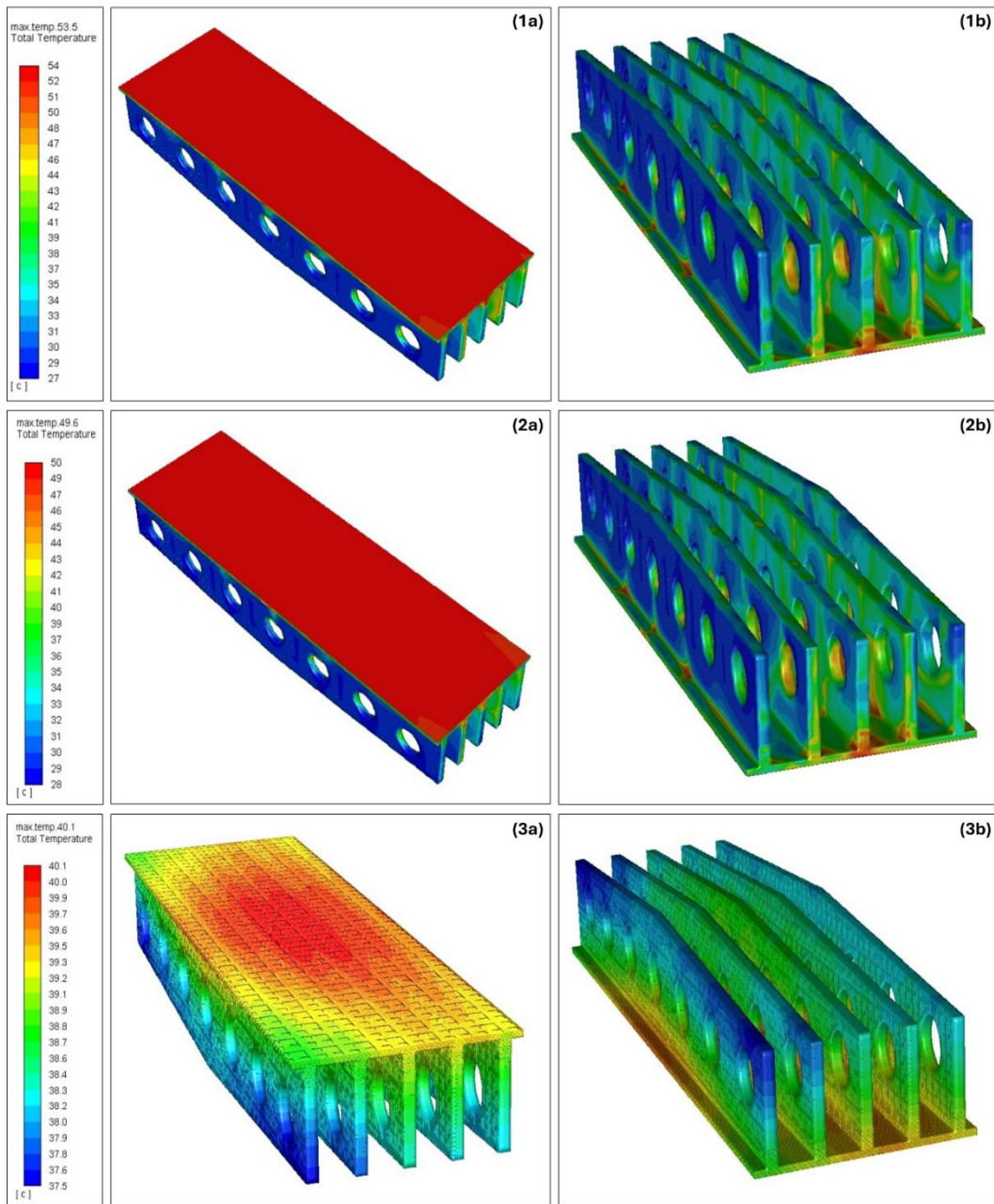
Figure 9. Temperature distribution of knuckled HS design under vertical air flow: 1: 1m/s, 2: 1.5 m/s, 3: 3 m/s, **a)** top, **b)** bottom

Another noteworthy result here is that although the inclined HS option showed poor performance at all flow rates and in the vertical flow direction, the inclined perforated HS option dropped to lower temperatures than the smooth HS at the 3 m/s flow rate option for the same flow rate. Similarly, although the inclined perforated HS provided the lowest temperatures at all rates in the vertical flow rate, it drew a less successful picture than the other two options in the horizontal flow.

Figure 10. Temperature distribution of knuckled with holes HS design under vertical air flow: 1: 1m/s, 2: 1.5 m/s, 3: 3 m/s, **a)** top, **b)** bottom.

As a result, if the dominant wind direction is horizontal, using the smooth HS appears to be the best option in all flows. Therefore, modifying the HS or opening it with holes negatively affects the heat transfer performance and its success in reducing the PV panel temperature decreases. In addition, if there is a dominant wind breeze in the vertical direction, the inclined and perforated HS design gives the lowest temperature values.

As a result of the HS simulations, the preferred HS geometry was the inclined and perforated HS option. According to the results obtained, the inclined perforated HS produced and used in the experimental phase was mounted on the back surface of the PV panel using thermal paste and temperature measurements were made from the solar panel surface. In Figure 11, the distribution of surface temperatures of two core PV panels with and without HSs under equal solar radiation conditions is observed. In the figure, it is observed that the temperature of the solar panel with a HS is 48.9 C and the temperature of the PV panel without a HS is 59.6 C. These values are very close to the results obtained in the simulations. This proves that the simulation results are consistent with the experimental results.
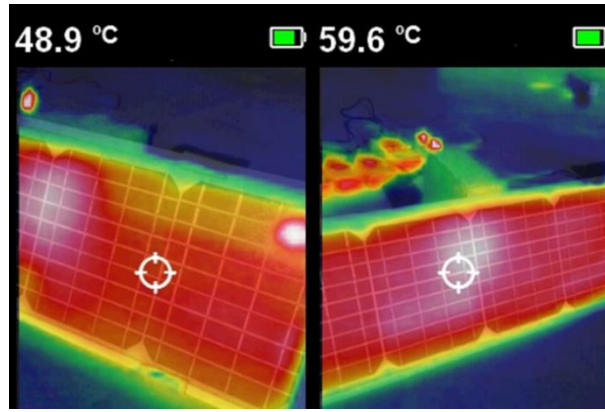
Figure 11. Peak temperatures the panels at 13:00.

Figure 12 shows the efficiency curves of PV panels without and with HSs according to the current voltage and radiation results obtained during the experimental study. It is clearly seen that the HS added during the measurements is stable at 16% efficiency. The PV panel without HS is seen to be operating at 13% efficiency. It has been experimentally proven that there is an efficiency difference of 15-22% throughout the day between these two applications.
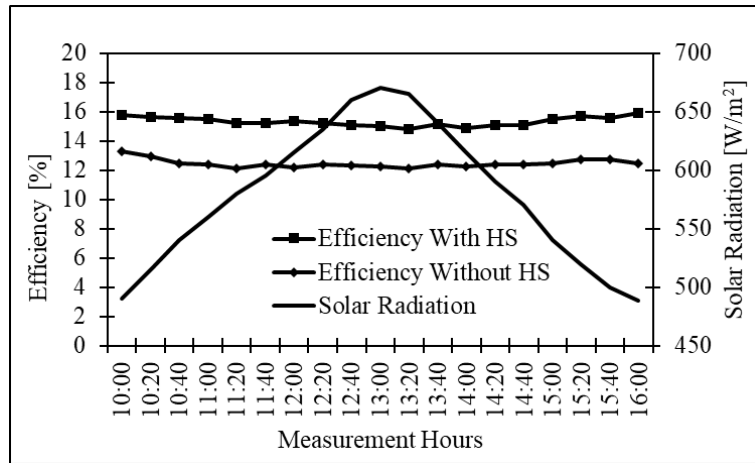

Figure 12. Efficiencies and solar radiation of the PV panels.

Figure 13 shows the voltage and current curves of PV panels with and without HSs during the measurement hours. It is observed that the current and voltage values peak between 12:00 and 13:00 in the middle of the day during the measurements. The reason why the voltage values are below the label values is that the radiation values in the region are below the standard test conditions radiation value of 1000 W/m^2.
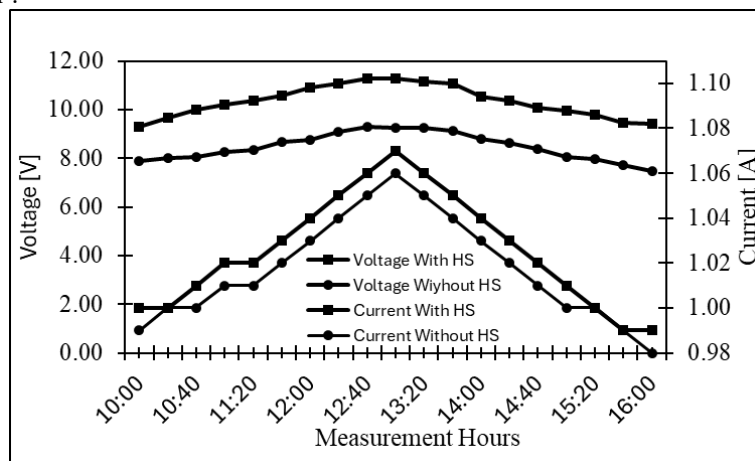

Figure 13. Voltage and current measurements with and without HS.

Similarly, Figure 13 shows the curves of the power values produced by both PV panels during the day. Here, it is seen that the difference between the power outputs is 15-22% in favor of the PV panel using the HS.
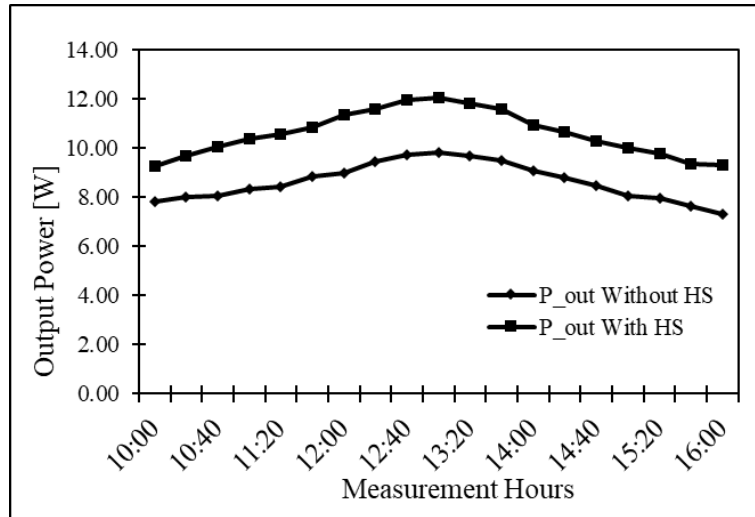
Figure 14. Output power values with and without heays sink.

Figure 15 shows the temperature difference between the two panels during the measurement hours. In the measurements made throughout the day, it is observed that the difference between the two panels is maintained at approximately 10C. When the obtained values are examined, it can be easily predicted that the temperatures of the panels to be installed in hot climates will reach high values and significantly affect efficiency. Therefore, it can be clearly predicted that much higher temperature differences can be achieved by applying a HS to the temperatures of the PV panels in hot climates.
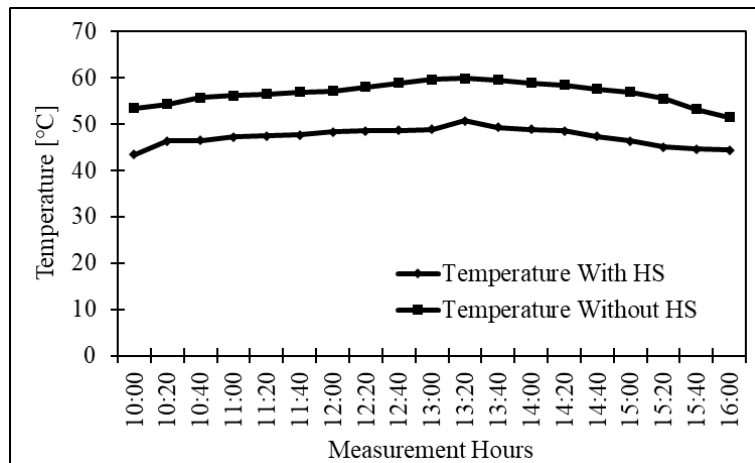

Figure 15. Temperature changes versus time of the PV panels.

When Figure 16 is examined, the efficiency change according to the temperature of silicon PV panels is seen according to Eq. 10. Accordingly, theoretically, when the ambient humidity and shading conditions are ignored, the PV panel temperature increases to 120 C, conversion efficiency, which is 17% in standard test conditions, decreases to 10%. The temperature increase will almost halve the operating efficiency of PV panels in hot climate regions where HS applications are not made and will also reduce the amount of electricity production.
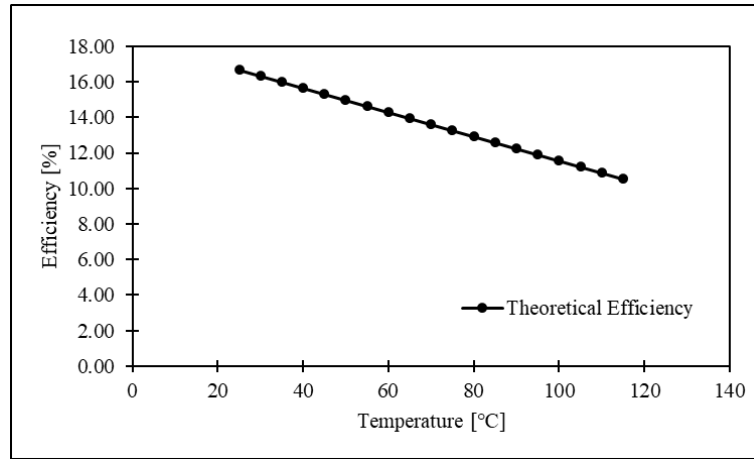
Figure 16. Theoretical efficiency decrease versus temperature.

4. Conclusion

During the field experiment, two identical PV panels were used. To enhance cooling performance, three design options were evaluated using ANSYS Fluent software, considering airflow velocity, solar radiation, and airflow direction. After reviewing the simulation results, the most promising design was manufactured and tested at Karabük University Campus. Temperature, voltage, and power values were recorded between 10:00 and 16:00 to calculate the efficiency of both panels. A thermal camera and four multimeters were used to record the surface temperature and power output of the PV panels at 20-minute intervals. The efficiency differences between the PV panel with and without a HS ranged from 15-22%.

For future work, two approaches could be taken. The first option involves conducting additional experiments with the base design, which is more economically feasible and easier to produce. The second option involves further analysis of the promising HS design, including cost analysis, to develop more efficient PV systems. In addition, it would be useful to try similar studies in different climate conditions and more advanced geometry.

Nomenclature

Symbols

T_o : temperature at zero efficiency [°C]
n_{eff} : calculated efficiency
β : temperature coefficient [1/K]
T_c : operating temperature [°C]
T_{reff} : reference temperature at reference efficiency
ρ : density [kg/m^3]
$\vec{v}$: velocity of fluid [m/s]
∇ : divergence
P : static pressure [kPa]

$\bar{\bar{\tau}}$: the stress tensor
ρg : gravitational body force
F : external body forces
μ : molecular viscosity
I : unit tense
u_m : mean velocity [m/s]
Re_L : Reynolds number

Abbreviations

PV : Photovoltaic
CFD : Computational Fluid Dynamics
a-Si : amorphous Silicon
c-Si : crystalline Silicon

References

[1]   Khudhur J, Akroot A, Al-Samari A. Experimental Investigation of Direct Solar Photovoltaics that Drives Absorption Refrigeration System. J Adv Res Fluid Mech Therm Sci 2023;106:116–35. https://doi.org/10.37934/arfmts.106.1.116135.
[2]   Atkin P, Farid MM. Improving the efficiency of photovoltaic cells using PCM infused graphite and aluminium fins. Sol Energy 2015;114:217–28. https://doi.org/10.1016/J.SOLENER.2015.01.037.
[3]   Bergman, Lavine, Incropera D. Fundamentals of Heat and Mass Transfer 7th Edition. 2003. https://doi.org/10.16309/j.cnki.issn.1007-1776.2003.03.004.
[4]   Akyavuz UD, Kayabasi E, Ozcan H. The effect of solar thermal energy storage on natural gas heating systems: An experimental and techno-economic investigation. Case Stud Therm Eng 2024;63:105287. https://doi.org/10.1016/J.CSITE.2024.105287.

[5]   Dawood TA, Barwari RRI, Akroot A. Solar Energy and Factors Affecting the Efficiency and Performance of Panels in Erbil/Kurdistan. Int J Heat Technol 2023;41:304–12. https://doi.org/10.18280/ijht.410203.

[6]   Beaucarne G. Silicon thin-film solar cells. Adv Optoelectron 2007;2007. https://doi.org/10.1155/2007/36970.

[7]   Yilmaz M, Kayabasi E, Akbaba M. Determination of the effects of operating conditions on the output power of the inverter and the power quality using an artificial neural network. Eng Sci Technol an Int J 2019. https://doi.org/10.1016/j.jestch.2019.02.006.

[8]   Eldin AH. A Review on Photovoltaic Solar Energy Technology and its Efficiency 2007.

[9]   Idoko L, Anaya-Lara O, McDonald A. Enhancing PV modules efficiency and power output using multi-concept cooling technique. Energy Reports 2018;4:357–69. https://doi.org/10.1016/j.egyr.2018.05.004.

[10]   Alami AH. Microstructural, optical and thermal characterization of synthetic clay as a passive cooling medium. Energy Convers Manag 2014;88:442–6. https://doi.org/10.1016/j.enconman.2014.08.053.

[11]   Özkul FB, Kayabasi E, Çelik E, Kurt H, Arcaklioğlu E. Investigating the Effects of Cooling Options on Photovoltaic Panel Efficiency : State of the Art and Future Plan. 2018 Int. Conf. Photovolt. Sci. Technol., IEEE Explore Digital Library; 2018, p. 1–6.

[12]   Sheikh Y, Jasim M, Qasim M, Qaisieh A, Hamdan MO, Abed F. Enhancing PV solar panel efficiency through integration with a passive Multi-layered PCMs cooling system: A numerical study. Int J Thermofluids 2024;23:100748. https://doi.org/10.1016/J.IJFT.2024.100748.

[13]   Hamed MH, Hassan H, Ookawara S, Nada SA. Performance comparative study on passively cooled concentrated photovoltaic (PV) using adsorption/desorption and heat sink cooling methods: Experimental investigations. Energy 2024;307:132700. https://doi.org/10.1016/J.ENERGY.2024.132700.

[14]   Rahimi M, Asadi M, Karami N, Karimi E. A comparative study on using single and multi header microchannels in a hybrid PV cell cooling. Energy Convers Manag 2015;101:1–8. https://doi.org/10.1016/j.enconman.2015.05.034.

[15]   Ebrahimi M, Rahimi M, Rahimi A. An experimental study on using natural vaporization for cooling of a photovoltaic solar cell. Int Commun Heat Mass Transf 2015;65:22–30. https://doi.org/10.1016/j.icheatmasstransfer.2015.04.002.

[16]   Al-Waeli AHA, Sopian K, Chaichan MT, Kazem HA, Hasan HA, Al-Shamani AN. An experimental investigation of SiC nanofluid as a base-fluid for a photovoltaic thermal PV/T system. Energy Convers Manag 2017;142:547–58. https://doi.org/10.1016/j.enconman.2017.03.076.

[17]   Global Solar Atlas n.d. https://globalsolaratlas.info/map.

[18]   Dubey S, Sarvaiya JN, Seshadri B. Temperature dependent photovoltaic (PV) efficiency and its effect on PV production in the world - A review. Energy Procedia 2013;33:311–21. https://doi.org/10.1016/j.egypro.2013.05.072.

[19]   Bayrak F, Oztop HF, Selimefendigil F. Experimental study for the application of different cooling techniques in photovoltaic (PV) panels. Energy Convers Manag 2020;212:112789. https://doi.org/10.1016/j.enconman.2020.112789.